

Representation Deficiency in Masked Language Modeling

Yu Meng^{1*} Jitin Krishnan² Sinong Wang² Qifan Wang² Yuning Mao² Han Fang² Marjan Ghazvininejad²
 Jiawei Han¹ Luke Zettlemoyer²

Abstract

Masked Language Modeling (MLM) has been one of the most prominent approaches for pretraining bidirectional text encoders due to its simplicity and effectiveness. One notable concern about MLM is that the special [MASK] symbol causes a discrepancy between pretraining data and downstream data as it is present only in pretraining but not in fine-tuning. In this work, we offer a new perspective on the consequence of such a discrepancy: We demonstrate empirically and theoretically that MLM pretraining allocates some model dimensions exclusively for representing [MASK] tokens, resulting in a representation deficiency for real tokens and limiting the pretrained model’s expressiveness when it is adapted to downstream data without [MASK] tokens. Motivated by the identified issue, we propose MAE-LM, which pre-trains the Masked Autoencoder architecture with MLM where [MASK] tokens are excluded from the encoder. Empirically, we show that MAE-LM improves the utilization of model dimensions for real token representations, and MAE-LM consistently outperforms MLM-pretrained models across different pretraining settings and model sizes when fine-tuned on the GLUE and SQuAD benchmarks.

1. Introduction

Pretraining text encoders to learn from bidirectional contexts has achieved enormous success in various natural language processing (NLP) tasks (Clark et al., 2020; Devlin et al., 2019; Liu et al., 2019). Masked Language Modeling (MLM) (Devlin et al., 2019) is among one of the most prominent pretraining approaches due to its conceptual simplicity and empirical effectiveness: By randomly masking a

portion of input tokens and training a Transformer encoder to predict the original content based on the remaining bidirectional contexts, the model learns robust representations that generalize well to diverse downstream tasks. Besides its broad impact in NLP, MLM has also been widely adopted for pretraining in other domains, such as images (Bao et al., 2022; Xie et al., 2022), videos (Tong et al., 2022; Wang et al., 2022) and graphs (Hou et al., 2022).

Despite its remarkable success, the effectiveness of MLM may be hindered by a discrepancy between pretraining and fine-tuning: The special [MASK] token occurs only in pre-training but not in downstream tasks. While a few previous studies (Clark et al., 2020; Yang et al., 2019) have attempted to address this issue, they end up proposing new training objectives instead of systematically investigating why and how such a discrepancy impacts the generalization of MLM-pretrained models.

In this work, we study the consequence of including [MASK] tokens in MLM pretraining by examining the learned token representation space. We empirically and theoretically show that [MASK] token representations exclusively occupy some model dimensions, thereby reducing the model capacity for representing real tokens. Such a representation deficiency issue may not be simply addressed by fine-tuning on downstream tasks: Those dimensions exclusively used for [MASK] tokens have not been pretrained to represent real tokens, and will have to be either trained from scratch on downstream data, raising the risk of overfitting (Hendrycks et al., 2019; Kumar et al., 2022), or become unused, resulting in a waste of model capacity.

To address the representation deficiency issue, we propose a simple text encoder pretraining method, MAE-LM, which conducts MLM pretraining based on the Masked Autoencoder architecture (He et al., 2022). Notably, [MASK] tokens are omitted from the encoder’s input so that the real token representations can utilize the entire model dimensions theoretically. An auxiliary decoder, which is used only in pretraining and not in fine-tuning, takes the encoder’s output representations and [MASK] positions to predict the original tokens. We demonstrate empirically that by excluding [MASK] tokens from the encoder, MAE-LM improves the utilization of model dimensions in pretraining and down-

* Work done during internship at Meta AI.¹University of Illinois at Urbana-Champaign {yumeng5, hanj}@illinois.edu

²Meta AI {jitinkrishnan, sinongwang, wqfcr, yuningm, hanfang, ghazvini, lsz}@meta.com

stream tasks. Under various standard pretraining settings and model sizes, MAE-LM achieves consistent and notable improvements over previous models pretrained by MLM and its variants on the GLUE and SQuAD benchmarks.

Our main contributions are as follows: (1) We investigate the token representation space trained by MLM, and identify a previously unknown representation deficiency issue when the pretrained model is applied to real data without [MASK] tokens. (2) Based on empirical and theoretical analyses, we explain why the representation deficiency issue occurs in the conventional MLM pretraining setup. (3) We propose a simple pretraining method MAE-LM that addresses the identified issue and improves the fine-tuning performance of previous MLM-pretrained models under different pretraining settings and model sizes. Our analyses and results also provide new perspectives to understand why certain pretraining methods (e.g., ELECTRA (Clark et al., 2020)) and adaptation methods (e.g., prompt-based fine-tuning (Gao et al., 2021; Schick & Schütze, 2021)) are advantageous, and may shed light on future research of MLM-style pretraining methods.

2. Analysis of Token Representations in MLM

2.1. Preliminaries

Transformer Encoder. Transformer encoders contain multiple Transformer layers, where each layer consists of two submodules, multi-head self-attention (MHSA) and feed-forward network (FFN). The self-attention mechanism uses queries \mathbf{Q} and keys \mathbf{K} to compute attention weights, and outputs a weighted sum of the values \mathbf{V} . MHSA performs self-attention in parallel over N heads as follows:

$$\text{Attn}(\mathbf{Q}, \mathbf{K}, \mathbf{V}) = \text{Softmax}\left(\frac{\mathbf{Q}\mathbf{K}^\top}{\sqrt{d_h}}\right)\mathbf{V},$$

$$\text{head}_h = \text{Attn}(\mathbf{X}\mathbf{W}_h^Q, \mathbf{X}\mathbf{W}_h^K, \mathbf{X}\mathbf{W}_h^V),$$

$$\text{MHSA}(\mathbf{X}) = \text{Concat}(\text{head}_1, \dots, \text{head}_N)\mathbf{W}^O,$$

where $\mathbf{X} \in \mathbb{R}^{n \times d}$ is the input representations to MHSA, n is the sequence length and d is the model dimension. d_h is the dimension of head h and is usually set to d/N . $\mathbf{W}_h^Q, \mathbf{W}_h^K, \mathbf{W}_h^V \in \mathbb{R}^{d \times d_h}$ and $\mathbf{W}^O \in \mathbb{R}^{d \times d}$ are learnable weight matrices. The outputs of MHSA are further passed to FFN which learns nonlinear transformations to derive the final outputs of the Transformer layer.

Masked Language Modeling (MLM). Given a text sequence $\mathbf{x} = [x_1, \dots, x_i, \dots, x_n]$, MLM randomly selects a set of token positions \mathcal{M} and replaces them with a special [MASK] symbol. The resulting partially masked sequence $\hat{\mathbf{x}} = [x_1, \dots, [\text{MASK}]_i, \dots, x_n]$ is then fed to the Transformer encoder θ which outputs the token representations $\mathbf{H} = [\mathbf{h}_1, \dots, \mathbf{h}_i, \dots, \mathbf{h}_n]$. Finally, the encoder θ is

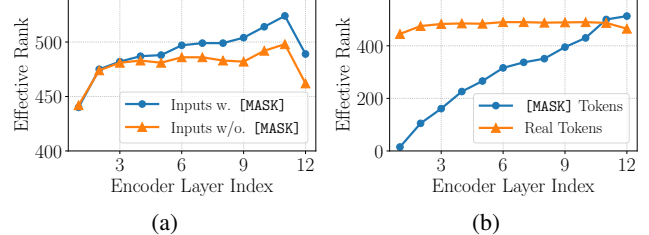


Figure 1: In an MLM-pretrained model, (a) some model dimensions are exclusively used for representing [MASK] tokens, resulting in a representation deficiency for modeling inputs without [MASK], especially in deeper layers; (b) the effective rank of [MASK] token representation space increases throughout Transformer layers.

trained to predict the original token out of the vocabulary \mathcal{V} at each masked position by minimizing the cross-entropy loss \mathcal{L}_{MLM} :

$$p_{\theta}(x_i|\hat{\mathbf{x}}) = \frac{\exp(\mathbf{e}_{x_i}^\top \mathbf{h}_i)}{\sum_{x' \in \mathcal{V}} \exp(\mathbf{e}_{x'}^\top \mathbf{h}_i)},$$

$$\mathcal{L}_{\text{MLM}} = \mathbb{E} \left(- \sum_{i \in \mathcal{M}} \log p_{\theta}(x_i|\hat{\mathbf{x}}) \right),$$

where \mathbf{e}_x refers to the embedding of token x .

2.2. Rank-Deficient Real Token Representations

MLM pretraining introduces a special [MASK] token to replace the token positions to be predicted, but such [MASK] tokens are usually absent from downstream task data. Therefore, to study the PLM’s capacity for downstream data representation, we examine the *real token* representation space trained with MLM. We are interested in the rank of the real token representation matrix $\mathbf{H}_{\mathcal{R}} \in \mathbb{R}^{n \times d}$ ($n \gg d$) where each row corresponds to the representation of a real token. Ideally, one would hope $\mathbf{H}_{\mathcal{R}}$ to have high column rank (*i.e.*, $\text{rank}(\mathbf{H}_{\mathcal{R}}) \approx d$) so that more model dimensions are effective for modeling real tokens. However, as we will show next, a portion of the model dimensions will be exclusively used for [MASK] token representations in MLM pretraining, so that $\mathbf{H}_{\mathcal{R}}$ is necessarily rank-deficient (*i.e.*, not all model dimensions are leveraged to represent real tokens).

Empirical Evidence. We evaluate the representation space of a pretrained 12-layer RoBERTa_{base} model (Liu et al., 2019) on the validation set of the pretraining corpus. We first apply 15% random masks to these input sequences (same as the pretraining setting), and obtain the token representation matrix $\mathbf{H}^l \in \mathbb{R}^{n \times d}$ ($n \approx 5 \times 10^6$, $d = 768$), which contains both real token and mask token representations, for each layer l in the pretrained RoBERTa model. We then feed the same input sequences in their original form (*i.e.*, without [MASK]) to the pretrained RoBERTa model and obtain the token representation matrix $\widetilde{\mathbf{H}}^l \in \mathbb{R}^{n \times d}$ which consists of

real token representations only. Comparing the rank of $\widetilde{\mathbf{H}}^l$ with \mathbf{H}^l gives insights about the change in representation capacity when adapting a pretrained MLM model to input sequences without [MASK].

Since numerical errors and small perturbations practically render any large matrix full-rank regardless of its actual rank, we compute the *effective rank* (Cai et al., 2021) of a matrix \mathbf{H} : We only consider \mathbf{H} ’s most significant components that account for the majority of the variance reflected by singular values. Given a threshold value τ , we define the τ -effective rank of \mathbf{H} as

$$\text{rank}_\tau(\mathbf{H}) = \arg \min_k \left(\frac{\sum_{i=1}^k \sigma_i^2}{\sum_{i=1}^d \sigma_i^2} \geq \tau \right),$$

where σ_i is the i th largest singular value of \mathbf{H} . For example, $\text{rank}_{0.9}(\mathbf{H}) = 10$ means that 90% of \mathbf{H} ’s variance can be captured with 10 dimensions.

Figure 1(a) shows $\text{rank}_{0.9}(\mathbf{H}^l)$ (Input w. [MASK]) and $\text{rank}_{0.9}(\widetilde{\mathbf{H}}^l)$ (Input w/o. [MASK]). It generally holds that $\text{rank}_{0.9}(\widetilde{\mathbf{H}}^l) < \text{rank}_{0.9}(\mathbf{H}^l)$, and the gap is more prominent in deeper layers. This demonstrates that some model dimensions are reserved for [MASK] token representations in almost all encoder layers, and these dimensions are not active when the input sequences consist of real tokens entirely. Such representation deficiencies for modeling real tokens become more severe in deeper layers where [MASK] token representations occupy more dimensions, as shown in Figure 1(b).

Theoretical Analysis. We theoretically validate the empirical observation above that MLM necessarily allocates a subspace for [MASK] token representations which is not contained by the real token representation subspace, so that the real token representations are rank-deficient.

Lemma 2.1 (Rank increase of [MASK] token representations in Transformer encoder). *The rank of [MASK] token representations will increase from the input layer to the output layer of an L -layer Transformer encoder trained with MLM (i.e., $\text{rank}(\mathbf{H}_\mathcal{M}^L) \gg \text{rank}(\mathbf{H}_\mathcal{M}^0)$).*

Proof. We first show that $\mathbf{H}_\mathcal{M}^L$ will be high-rank in a well-trained MLM model and then show that $\mathbf{H}_\mathcal{M}^0$ is necessarily low-rank, and thus the statement holds.

As shown in Eq. (1), the output token probability distributions at masked positions are computed from the encoder’s output representations $\mathbf{H}_\mathcal{M}^L \in \mathbb{R}^{m \times d}$ and token embeddings $\mathbf{E} \in \mathbb{R}^{|\mathcal{V}| \times d}$. Denote the true log probability distributions of the masked token prediction task as $\mathbf{T} \in \mathbb{R}^{m \times |\mathcal{V}|}$:

$$\mathbf{T} = \begin{bmatrix} \log p(x_1|\hat{x}_1) & \log p(x_2|\hat{x}_1) & \cdots & \log p(x_{|\mathcal{V}|}|\hat{x}_1) \\ \log p(x_1|\hat{x}_2) & \log p(x_2|\hat{x}_2) & \cdots & \log p(x_{|\mathcal{V}|}|\hat{x}_2) \\ \vdots & \vdots & \ddots & \vdots \\ \log p(x_1|\hat{x}_m) & \log p(x_2|\hat{x}_m) & \cdots & \log p(x_{|\mathcal{V}|}|\hat{x}_m) \end{bmatrix},$$

then $\mathbf{H}_\mathcal{M}^L$ and \mathbf{E} are trained to approximate \mathbf{T} with a row shift (due to the softmax normalization) (Yang et al., 2018):

$$\mathbf{H}_\mathcal{M}^L \mathbf{E}^\top \approx \mathbf{T} + \mathbf{c} \mathbf{1}^\top, \quad (2)$$

where $\mathbf{c} \in \mathbb{R}^m$ contains the shifting constant added to each row, and $\mathbf{1} \in \mathbb{R}^{|\mathcal{V}|}$ is a vector of all ones.

It is shown in (Yang et al., 2018) that the true probability distribution \mathbf{T} is high-rank (as high as $|\mathcal{V}|$) due to the complexity of natural language. Since $\text{rank}(\mathbf{H}_\mathcal{M}^L \mathbf{E}^\top) \leq \min\{\text{rank}(\mathbf{H}_\mathcal{M}^L), \text{rank}(\mathbf{E})\}$, both $\mathbf{H}_\mathcal{M}^L$ and \mathbf{E} need to be high-rank to achieve a good approximation of $\mathbf{T} + \mathbf{c} \mathbf{1}^\top$.

Next, we show $\mathbf{H}_\mathcal{M}^0$ is low-rank. $\mathbf{H}_\mathcal{M}^0$ is the sum of token embeddings and position embeddings at masked positions:

$$\mathbf{H}_\mathcal{M}^0 = \mathbf{1} \mathbf{e}_{[\text{MASK}]}^\top + \mathbf{P},$$

where $\mathbf{e}_{[\text{MASK}]} \in \mathbb{R}^d$ is the [MASK] token embedding, and $\mathbf{P} \in \mathbb{R}^{m \times d}$ is the position embeddings.

Since we have $\text{rank}(\mathbf{1} \mathbf{e}_{[\text{MASK}]}^\top + \mathbf{P}) \leq \text{rank}(\mathbf{1} \mathbf{e}_{[\text{MASK}]}^\top) + \text{rank}(\mathbf{P}) = \text{rank}(\mathbf{P}) + 1$, we only need to show \mathbf{P} is low-rank. Previous studies (He et al., 2021b; Ke et al., 2021) have identified that position embeddings \mathbf{P} and token embeddings \mathbf{E} encode disjoint information, and are learned in separate subspaces of \mathbb{R}^d . Therefore, $\text{rank}(\mathbf{P}) \leq d - \text{rank}(\mathbf{E})$. We also showed that \mathbf{E} must be high-rank to satisfy Eq. (2), and thus \mathbf{P} is necessarily low-rank. Finally, $\mathbf{H}_\mathcal{M}^0$ is also low-rank as $\text{rank}(\mathbf{H}_\mathcal{M}^0) \leq \text{rank}(\mathbf{P}) + 1$. \square

Remark. Lemma 2.1 corresponds to the empirical observation in Figure 1(b), and can be intuitively interpreted as a necessary consequence of the [MASK] token contextualization process in Transformers: The [MASK] representations at the input layer are context-free, and they need to aggregate contextual information from other tokens in the sequence for predicting the original word, resulting in an increase in the information content of [MASK] token representations. We also note that the rank increase statement does not necessarily apply to real token representations. This is because MLM does not directly train the real token representations (e.g., the training objective in Eq. (2) does not apply to real token positions¹).

Based on Lemma 2.1, we proceed to prove that $\mathbf{H}_\mathcal{M}^l$ occupies a different subspace that is not contained by the subspace of $\mathbf{H}_\mathcal{R}^l$, resulting in deficient representations for real tokens.

Theorem 2.2 (Rank deficiency of real token representations). *There exists some layer l in the Transformer encoder*

¹Some MLM training settings adopt a trick that keeps 10% of [MASK] as original tokens and randomly replaces another 10% of [MASK] with other tokens. Even with this trick, the training signals on real token representations are scarce. Furthermore, later studies (Wettig et al., 2022) report that this trick is not necessary—training exclusively on [MASK] positions performs well.

where the real token representation $\mathbf{H}_{\mathcal{R}}^l$ is rank-deficient. In particular, the row space of $\mathbf{H}_{\mathcal{R}}^l$ does not contain the row space of [MASK] token representation $\mathbf{H}_{\mathcal{M}}^l$.

Proof. We provide a proof sketch below. Detailed proofs can be found in Appendix A. We prove the statement by contradiction: Suppose that the row space of $\mathbf{H}_{\mathcal{R}}^l \in \mathbb{R}^{n \times d}$ contains the row space of $\mathbf{H}_{\mathcal{M}}^l \in \mathbb{R}^{m \times d}$, then we have

$$\mathbf{H}_{\mathcal{M}}^l = \mathbf{U} \mathbf{H}_{\mathcal{R}}^l, \quad \mathbf{U} \in \mathbb{R}^{m \times n}. \quad (3)$$

We show that under this assumption, $\mathbf{H}_{\mathcal{M}}^l$ will converge exponentially (with l) to a rank-1 matrix, which contradicts with Lemma 2.1.

We adopt a similar approach as (Dong et al., 2021) to study the following residual \mathbf{R}^l which measures the difference between $\mathbf{H}_{\mathcal{R}}^l$ and a rank-1 matrix:

$$\mathbf{R}^l = \mathbf{H}_{\mathcal{R}}^l - \mathbf{1} \mathbf{h}^\top, \quad \mathbf{h} = \arg \min_{\mathbf{x}} \|\mathbf{H}_{\mathcal{R}}^l - \mathbf{1} \mathbf{x}^\top\|.$$

Based on the self-attention formula and the assumption in Eq. (3), we can derive a bound for the norm of \mathbf{R}^l as a function of \mathbf{R}^{l-1} :

$$\|\mathbf{R}^l\|_{1,\infty} \leq 4\epsilon \|\mathbf{R}^{l-1}\|_{1,\infty}^3,$$

where $\|\cdot\|_{1,\infty}$ denotes the geometric mean of ℓ_1 and ℓ_∞ norm, and

$$\epsilon = \left\| \frac{\mathbf{W}^Q \mathbf{W}^{K^\top}}{\sqrt{d}} \right\|_1 \|\mathbf{W}^V \mathbf{W}^O\|_{1,\infty} \|\mathbf{U}\|_\infty (1 + \|\mathbf{U}\|_\infty).$$

This shows that $\|\mathbf{R}^l\|_{1,\infty}$ converges exponentially with l to zero, and thus $\mathbf{H}_{\mathcal{R}}^l$ converges exponentially with l to a rank-1 matrix. We also have $\text{rank}(\mathbf{H}_{\mathcal{M}}^l) \leq \text{rank}(\mathbf{H}_{\mathcal{R}}^l)$ as the row space of $\mathbf{H}_{\mathcal{M}}^l$ is contained by the row space of $\mathbf{H}_{\mathcal{R}}^l$. Hence, $\mathbf{H}_{\mathcal{M}}^l$ will also converge exponentially to a rank-1 matrix, which contradicts with Lemma 2.1. Therefore, the statement holds. \square

Remark. Theorem 2.2 demonstrates that at least some [MASK] token representations and real token representations need to be linearly independent so that the rank of $\mathbf{H}_{\mathcal{M}}^l$ may increase through encoder layers. As a result, the real token representation $\mathbf{H}_{\mathcal{R}}^l$ cannot utilize the entire model dimensions and is prone to rank deficiency.

3. MAE-LM: Masked Autoencoders for MLM

To address the representation deficiency issue in MLM, we propose a simple framework MAE-LM, which pretrains bidirectional Transformer encoders using the MLM objective, but based on the Masked Autoencoder (He et al., 2022) structure. An overview of MAE-LM is shown in Figure 2.

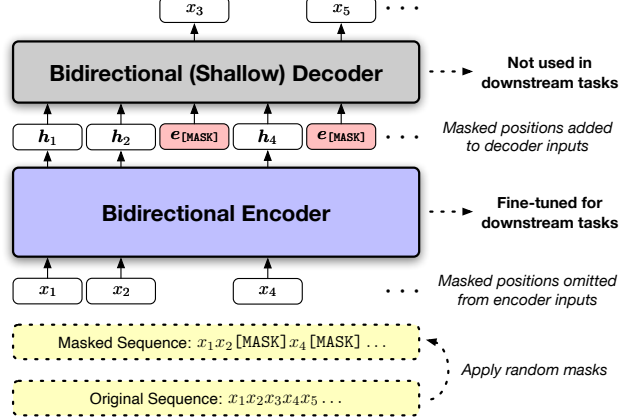


Figure 2: Overview of MAE-LM. Masked positions are omitted from encoder inputs so that the encoder purely models real tokens. A shallow decoder takes the encoder’s output representations and masked positions to predict the original tokens. After pretraining, only the encoder (but not the decoder) is fine-tuned for downstream tasks.

Excluding [MASK] from the Encoder. An important design in MAE-LM is that [MASK] tokens are excluded from the encoder inputs so that no model dimensions will be used to represent [MASK] tokens. Hence, the representations of real tokens $\mathbf{H}_{\mathcal{R}}$ can theoretically utilize the entire space \mathbb{R}^d , which addresses the representation bottleneck in conventional MLM pretraining. Specifically, given a masked sequence $\hat{\mathbf{x}} = [x_1, \dots, \text{[MASK]}_i, \dots, x_n]$ and let \mathcal{M} denote the set of masked positions, the encoder’s input sequence \mathbf{H}^0 consists of the sum of token embeddings \mathbf{e}_{x_i} and position embeddings \mathbf{p}_i at real token positions $i \notin \mathcal{M}$:

$$\mathbf{H}^0 = \{\mathbf{h}_i^0\}_{i \notin \mathcal{M}}, \quad \mathbf{h}_i^0 = \mathbf{e}_{x_i} + \mathbf{p}_i.$$

Decoder Configuration. In order to predict the original tokens at masked positions, the encoder’s output token representations \mathbf{H}^L are further passed to an auxiliary bidirectional decoder. While standard Transformer decoders perform unidirectional self-attention (and cross-attention to encoder outputs) for autoregressive decoding, our decoder performs bidirectional self-attention (same as the encoder). It is called a decoder as it takes encoded representations as input and outputs tokens. The decoder’s input sequence $\widehat{\mathbf{H}}^0$ needs to include the [MASK] token embedding $\mathbf{e}_{\text{[MASK]}}$ and position embeddings \mathbf{p}_i so that the decoder is aware of the positions to be predicted:

$$\widehat{\mathbf{H}}^0 = \{\widehat{\mathbf{h}}_i^0\}_{1 \leq i \leq n}, \quad \widehat{\mathbf{h}}_i^0 = \begin{cases} \mathbf{e}_{\text{[MASK]}} + \mathbf{p}_i & i \in \mathcal{M} \\ \mathbf{h}_i^L + \mathbf{p}_i & i \notin \mathcal{M} \end{cases}.$$

The decoder’s output representations will be trained with the MLM objective shown in Eq. (1). Since the decoder includes [MASK] tokens, it is subject to the representation

deficiency for modeling real tokens as analyzed in Section 2. Therefore, the decoder is *not* used in fine-tuning on downstream tasks. The decoder is made to be shallow (the decoder depth is $1/6 - 1/3$ of the encoder in our experiments) not only for pretraining efficiency, but also to push the encoder to learn robust token representations—if the decoder is too strong, it alone may learn the MLM task well without requiring good encoder representations H^L .

Despite using an additional decoder in pretraining, MAE-LM’s pretraining time cost is roughly equal to that of conventional MLM pretraining (*e.g.*, RoBERTa). This is because the exclusion of [MASK] tokens from the encoder practically reduces its input sequence length (*e.g.*, 15% random masks shorten the encoder’s input length by 15%), bringing down the encoder’s computation cost.

4. Experiments

4.1. Pretraining and Evaluation Setup

Pretraining Settings. We evaluate MAE-LM under three standard pretraining settings: *base*, *base++*, and *large++*. All settings use the MLM objective for pretraining and we do not use any sequence-level tasks.

The *base* setting follows BERT_{base} (Devlin et al., 2019) pre-training which uses Wikipedia and BookCorpus (Zhu et al., 2015) (16GB of texts) as the pretraining corpora. The encoder architecture is a 12-layer Transformer, and the model dimension is 768. We train both absolute and relative position embeddings (Raffel et al., 2019) in the encoder. The decoder is a 4-layer Transformer with the same model dimensions as the encoder. Since the decoder is not used in downstream tasks, MAE-LM’s encoder can be fairly compared with previous 12-layer base-sized models. The model is trained for 125K steps with 2,048 sequences per batch, which amounts to 256M samples in total. The maximum input sequence length is 512 tokens. The vocabulary is constructed with Byte Pair Encoding (BPE) (Sennrich et al., 2015) and consists of 32,768 *uncased* subword units.

The *base++* setting follows RoBERTa (Liu et al., 2019) pretraining which extends the *base* setting by incorporating larger pretraining corpora and training the same model architecture for longer. Specifically, the following corpora are used along with Wikipedia and BookCorpus: OpenWebText (Gokaslan & Cohen, 2019), CC-News (Liu et al., 2019), and STORIES (Trinh & Le, 2018). This expands the pretraining corpora to contain 160GB texts. The model is trained for 2M steps with 2,048 sequences per batch, which amounts to 4B samples in total. The *base++* setting also upgrades the vocabulary by using *cased* subword units and expanding the vocabulary size to 64,000 (Bao et al., 2020).

The *large++* setting extends the *base++* setting by scaling

up the encoder architecture to 24 layers and 1,024 model dimensions. The decoder is still a 4-layer Transformer with the same model dimensions as the encoder. Due to the high cost of training large models, we train for 1M steps (half of the *base++* setting) with 2,048 sequences per batch, which amounts to 2B samples in total. Note that this is also half of the pretraining data used in RoBERTa (Liu et al., 2019) and BART (Lewis et al., 2020).

Downstream Tasks and Fine-Tuning. We evaluate the pretrained models on the GLUE (Wang et al., 2018) and SQuAD 2.0 (Rajpurkar et al., 2016) benchmarks. The details about GLUE tasks can be found in Appendix B. We adopt standard fine-tuning as in BERT (Devlin et al., 2019) and RoBERTa (Liu et al., 2019). The hyperparameter search space for fine-tuning can be found in Appendix D. All reported fine-tuning results are the medians of five random seeds on GLUE and SQuAD, following previous studies (Liu et al., 2019).

Baselines. We compare with various baselines pretrained by MLM (and variants of MLM) under each setting. The baseline results, unless marked by “(Ours)”, are taken from the original papers except the result of BERT_{base} which is reported by (Bao et al., 2020). To eliminate the performance difference due to implementation details and computation environment, we also pretrain and fine-tune RoBERTa (the most important baseline) under exactly the same *base* pretraining setting with MAE-LM, which is denoted with “RoBERTa (Ours)”.

Implementation Details. Our implementation is built on the fairseq (Ott et al., 2019) open-source library. More implementation details are mentioned in Appendix C.

4.2. Overall Results

Table 1 shows the results under the three pretraining settings on the GLUE and SQuAD 2.0 benchmarks. Overall, MAE-LM outperforms previous models pretrained by MLM and its variants. Notably, the gains of MAE-LM over RoBERTa (the standard MLM pretrained model) are quite consistent across tasks and pretraining settings. Under the *large++* setting, MAE-LM is pretrained on half of RoBERTa’s data, and still performs comparably or better than RoBERTa.

Pretraining Efficiency. In Figure 3, we illustrate MAE-LM_{base}’s fine-tuning performance when pretrained for different amounts of time. MAE-LM takes slightly more time than RoBERTa when trained on the same amount of data, but to reach RoBERTa’s MNLI accuracy, MAE-LM only needs about 40% of its pretraining time.

4.3. Ablation Studies

We create several groups of ablations to study the important components in MAE-LM. The results are shown in Table 2.

Table 1: Standard single-task, single-model fine-tuning results (medians over five random seeds) evaluated on GLUE and SQuAD 2.0 development sets. Results not available in prior research are marked with “–”. We use Spearman correlation for STS, Matthews correlation for CoLA, and accuracy for the other tasks on GLUE. The “AVG” column contains the averaged results across the eight GLUE tasks. All baseline results are taken from public reports unless marked with (Ours).

Model	GLUE (Single-Task)								SQuAD 2.0		
	MNLI-(m/mm)	QQP	QNLI	SST-2	CoLA	RTE	MRPC	STS-B	AVG	EM	F1
<i>base</i> setting: 12-layer, 768-dimensional Transformer model trained on Wikipedia & Book Corpus (16GB)											
BERT (Devlin et al., 2019)	84.5/-	91.3	91.7	93.2	58.9	68.6	87.3	89.5	83.1	73.7	76.3
ALBERT (Lan et al., 2020)	81.6/-	–	–	90.3	–	–	–	–	–	77.1	80.0
UniLMv2 (Bao et al., 2020)	86.1/86.1	–	–	93.2	–	–	–	–	–	80.9	83.6
TUPE (Ke et al., 2021)	86.2/86.2	91.3	92.2	93.3	63.6	73.6	89.9	89.2	84.9	–	–
RoBERTa (Liu et al., 2019)	84.7/-	–	–	92.7	–	–	–	–	–	–	79.7
RoBERTa (Ours)	85.9/85.8	91.6	92.3	93.7	64.3	75.5	88.7	89.5	85.2	78.3	81.5
MAE-LM	87.2/87.1	91.6	92.9	93.8	63.1	79.1	90.2	90.9	86.1	81.1	84.1
<i>base++</i> setting: 12-layer, 768-dimensional Transformer model trained on larger pretraining corpora (160GB)											
ALBERT (Lan et al., 2020)	82.4/-	–	–	92.8	–	–	–	–	–	76.3	79.1
RoBERTa (Liu et al., 2019)	87.6/-	91.9	92.8	94.8	63.6	78.7	90.2	91.2	86.4	80.5	83.7
UniLMv2 (Bao et al., 2020)	88.5/-	91.7	93.5	95.1	65.2	81.3	91.8	91.0	87.1	83.3	86.1
MAE-LM	89.1/89.1	91.7	93.8	95.1	65.9	85.2	90.2	91.6	87.8	83.5	86.5
<i>large++</i> setting: 24-layer, 1024-dimensional Transformer model trained on larger pretraining corpora (160GB)											
BART (Lewis et al., 2020)	89.9/90.1	92.5	94.9	96.6	62.8	87.0	90.4	91.2	88.2	86.1	89.2
RoBERTa (Liu et al., 2019)	90.2/90.2	92.2	94.7	96.4	68.0	86.6	90.9	92.4	88.9	86.5	89.4
MAE-LM	90.4/90.6	92.2	95.1	96.2	68.7	88.8	90.7	92.1	89.3	87.0	89.8

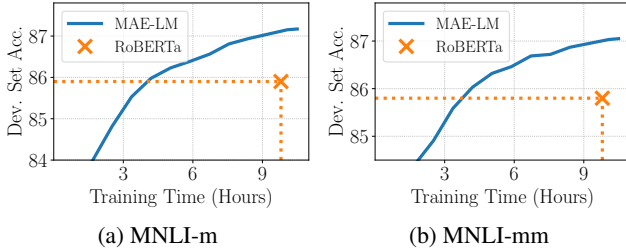


Figure 3: MNLI development set accuracy by fine-tuning intermediate MAE-LM_{base} checkpoints at different time steps. We also mark the pretraining time and final performance of RoBERTa (Ours). Training is conducted on 64 A100 GPUs.

Handling [MASK]. MAE-LM excludes [MASK] tokens from encoder’s inputs. We compare with other ways of handling [MASK] tokens in the encoder: (1) including [MASK] in encoder’s inputs without using the decoder, which is the standard MLM (enc. w. [MASK], no dec.); (2) including [MASK] in encoder’s inputs and using the same decoder (enc. w. [MASK]); (3) including [MASK] in encoder’s inputs but resetting [MASK] token positions to the [MASK] token embedding $e_{[MASK]}$ in decoder’s inputs (enc. w. [MASK], dec. resets [MASK]); and (4) randomly replacing [MASK] tokens in encoder’s inputs with other real tokens sampled from the vocabulary (random replace w. real token). Comparing (2) with (1), we validate that using the additional decoder is not the main reason for the performance gain. Comparing (3) with (2), one can see that when [MASK] is present in the encoder, resetting the [MASK]

Table 2: Ablations evaluated with GLUE average scores. The setting of MAE-LM_{base} is: enc. w/o. [MASK]; aligned position encoding w. relative position encoding; bi. self-attention; 4 layer, 768 dimension.

Group	Setting	GLUE
Original	MAE-LM _{base}	86.1
Handling [MASK]	enc. w. [MASK], no dec. (<i>i.e.</i> , MLM)	85.2
	enc. w. [MASK]	85.1
	enc. w. [MASK], dec. resets [MASK]	85.9
	random replace w. real token	85.1
Position Encoding	misaligned position encoding	86.0
	no relative position encoding	86.1
Decoder Attention	bi. self-attention + cross-attention	85.4
	uni. self-attention + cross-attention	85.5
	cross-attention	86.0
Decoder Size	2 layer, 768 dimension	85.8
	6 layer, 768 dimension	84.8
	4 layer, 512 dimension	85.8
	4 layer, 1024 dimension	85.5

token embeddings in the decoder helps. This validates our analysis in Theorem 2.2 that the rank increase of [MASK] token representations is the main cause of representation deficiency, and preventing [MASK] token representations in the encoder from being explicitly trained is one way to mitigate the issue, though it is slightly worse than not including [MASK] in the encoder at all. Comparing (4) with (2), we demonstrate that replacing [MASK] tokens with random real tokens, though avoiding the representation deficiency

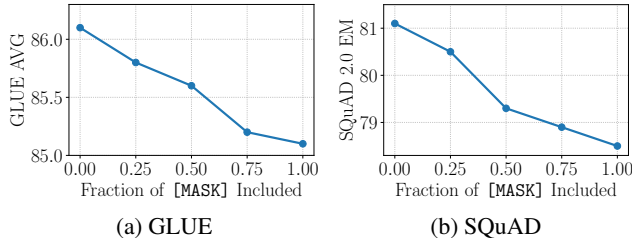


Figure 4: GLUE average scores and SQuAD EM scores when different fractions of [MASK] tokens are included in the input sequences to the encoder of MAE-LM_{base}.

problem, worsens the context quality in pretraining. On balance, it does not yield better results than MLM.

Position Encoding. MAE-LM aligns the position encoding based on each token’s position in the original sequence so that the position indices of masked positions are skipped. MAE-LM also uses relative position encoding (Raffel et al., 2019). We create two ablations regarding choices of position encoding: (1) apply consecutive position encoding that does not reflect the masked positions (misaligned position encoding); and (2) remove the relative position encoding from MAE-LM (no relative position encoding). Overall, the variations in position encoding do not result in notable performance differences.

Decoder Attention. MAE-LM uses bidirectional self-attention in the decoder. We compare with other decoder attention configurations: (1) additionally use cross-attention to encoder’s output representations (bi. self-attention + cross-attention); (2) use unidirectional self-attention and cross-attention for autoregressive decoding of the entire sequence, similar to BART (Lewis et al., 2020) (uni. self-attention + cross-attention); and (3) only use cross-attention (cross-attention). Only using bidirectional self-attention in the decoder is simple and performs better than other settings.

Decoder Size. MAE-LM uses a 4-layer decoder with the same dimensionality (768) as the encoder. We experiment with other decoder sizes (when the decoder’s dimension is different from the encoder, we add a linear projection between the encoder’s output and the decoder’s input): (1) 2-layer, 768 dimension; (2) 6-layer, 768 dimension; (3) 4-layer, 512 dimension; and (4) 4-layer, 1024 dimension. Overall, using a relatively small decoder yields good results.

Gradual Transition from MAE-LM to Standard MLM. To further examine the empirical benefits of excluding [MASK] tokens from MAE-LM’s encoder, we create a set of “stepping stones” between MAE-LM and standard MLM as follows: Out of all [MASK] tokens in the sequence \hat{x} , we include a fraction (δ) of them in the encoder’s input sequence. The rest ($1 - \delta$) of [MASK] tokens are excluded from the encoder’s input and added to the decoder’s input. Then $\delta = 0$ represents MAE-LM, and $\delta = 1$ refers to the

Table 3: Effective rank of encoder’s token representations by RoBERTa and MAE-LM after pretraining and after fine-tuning on MNLI and SQuAD 2.0.

Model	Pretrained	MNLI	SQuAD 2.0
RoBERTa (Ours)	462	149	103
MAE-LM	491	211	260

standard MLM². Figure 4 illustrates the fine-tuning performance changes on GLUE and SQuAD as we transition from MAE-LM to standard MLM. There is a clear trend that including a higher portion of [MASK] tokens in the encoder degrades its performance.

4.4. MAE-LM Improves Model Dimension Utilization

To further validate the effectiveness of MAE-LM in improving the utilization of model dimensions for representing real tokens, we compute the 0.9-effective rank of the encoder’s token representations $\text{rank}_{0.9}(\mathbf{H}^L)$ after pretraining (evaluated on the validation set of the pretraining corpus) and after further fine-tuning on MNLI and SQuAD 2.0 (evaluated on their validation sets). The comparison between RoBERTa and MAE-LM is shown in Table 3. Notably, MAE-LM results in a higher effective rank of real token representations than RoBERTa after pretraining, and such an advantage holds in downstream tasks after fine-tuning. This highlights the importance of addressing the representation deficiency issue in pretraining: The model dimensions used for representing [MASK] tokens in MLM pretraining may not be easily leveraged to model real tokens in fine-tuning as they have not been pretrained for such purposes.

5. Related Work

Language Model Pretraining. There have been various pretraining methods proposed for different purposes: Standard autoregressive language modeling (Brown et al., 2020; Radford et al., 2018; 2019) is commonly used to pretrain generative models that excels in text generation; MLM (Devlin et al., 2019; Liu et al., 2019) is prominently used to pretrain bidirectional text encoders to achieve superior performance for language understanding; Other language modeling objectives (Lewis et al., 2020; Raffel et al., 2019) are designed to build sequence-to-sequence models that serve as both text generators and text encoders. As one of the most prominent pretraining approaches, MLM has stimulated many follow-up developments for pretraining bidirectional encoders (Bao et al., 2020; Clark et al., 2020; He et al., 2021b; Joshi et al., 2019; Lan et al., 2020; Meng et al., 2021; 2022; Sanh et al., 2019; Yang et al., 2019). Remarkably, the

²Although standard MLM does not have the decoder, the fine-tuning results of $\delta = 1$ are very similar to RoBERTa (Ours).

idea of MLM has also proven to be highly generalizable to different domains (Bao et al., 2022; Dosovitskiy et al., 2021; Hou et al., 2022; Tong et al., 2022; Wang et al., 2022; Xie et al., 2022) and led to developments of unified pretraining frameworks for different modalities (Baevski et al., 2022). Given the broad impact of MLM, our analyses of representation deficiency in MLM may provide insights for future developments of pretraining algorithms in various fields.

Study of Pretrained Models’ Representations. The powerful language representations learned by pretrained models have driven a series of studies to understand how linguistic knowledge is captured by the Transformer encoder through pretraining. Previous work studying the token representations in pretrained encoders has found that deeper layers tend to generate more contextualized token representations (Ethayarajh, 2019), and these representations encode syntax structures (Goldberg, 2019; Hewitt & Manning, 2019) and fine-grained word senses (Coenen et al., 2019), offering supporting evidence for the effectiveness of pretrained models in downstream tasks. The success of learning such linguistic patterns is usually attributed to the multi-head self-attention mechanism which can automatically learn to extract useful features through pretraining (Clark et al., 2019). Furthermore, different types of linguistic information are shown to be represented in a hierarchical way from shallower to deeper layers, reflecting the traditional NLP pipeline (Tenney et al., 2019a;b). There have also been prior efforts that investigate the limitations of pretrained models’ representations. It has been revealed that the contextualized embedding space learned by pretrained models is generally anisotropic (Cai et al., 2021; Li et al., 2020) and is subject to a degeneration problem that token representations tend to be distributed into a narrow cone (Gao et al., 2019). In this work, we investigate a previously unknown issue regarding MLM-pretrained models’ representations which hinders the model’s expressiveness on real sequences without [MASK] tokens. Our findings contribute a new perspective to understanding the limitations of representations in pretrained models.

6. Discussions and Conclusion

Discussions. Since the advent of BERT (Devlin et al., 2019), there have been numerous developments in new pretraining and fine-tuning methods aiming to improve the effectiveness of pretrained models in downstream tasks. The advantages of these proposed methods, however, are mostly demonstrated via empirical evidence alone, and our understanding of why certain methods are better than the others remains limited. Our analyses in this work may advance the understanding of the benefits of some prominent methods: ELECTRA (Clark et al., 2020) fills [MASK] positions with real tokens; therefore, the encoder does not suffer from the

representation deficiency issue. Different from the ablation in Section 4.3 where we randomly sample real tokens to fill [MASK], ELECTRA employs an MLM model to sample replaced tokens which are generally plausible alternatives to the original tokens, thus better preserving the contexts in pretraining. These designs may help partially explain the effectiveness of ELECTRA. Prompt-based methods (Gao et al., 2021; Schick & Schütze, 2021) adapt pretrained MLM models to downstream tasks by creating prompt templates that convert the target task into a masked token prediction problem. This helps mitigate the representation deficiency issue that occurs in standard fine-tuning of MLM models as [MASK] tokens are also introduced into downstream data, resulting in more model dimensions being utilized.

Limitations and Ethical Considerations. The focus of our work is on MLM and our analyses do not apply to other pretraining settings not using [MASK] tokens (e.g., autoregressive pretraining). Empirically, we mainly compare with models pretrained by MLM and its simple variants, while state-of-the-art models usually need to combine multiple pretraining strategies (He et al., 2021a).

Despite their remarkable performance, pretrained models have been shown to come with risks such as exacerbating harmful biases (Bender et al., 2021; Bommasani et al., 2021). In our experiments, we follow the standard pretraining settings (e.g., data preparation, collection and preprocessing), and we expect more well-documented and filtered text corpora (Dodge et al., 2021), as well as future developments of harm reduction techniques (Liang et al., 2021) may help mitigate the ethical concerns about pretrained models.

Conclusion and Future Work. In this work, we investigate the discrepancy caused by [MASK] tokens in MLM pretraining and demonstrate for the first time that this will necessarily result in real token representations being rank-deficient, thus limiting the model’s expressiveness on real data without [MASK]. We propose a simple method MAE-LM that excludes [MASK] tokens from the encoder in pretraining to address the representation deficiency issue. We empirically show that MAE-LM improves the utilization of model dimensions for representing real tokens in pretraining and downstream tasks. MAE-LM consistently outperforms MLM-pretrained models on the GLUE and SQuAD benchmarks across multiple pretraining settings and model sizes.

Our proposed MAE-LM method is certainly not the only solution to address the identified issue. Promising future directions may include: designing regularization methods in pretraining that prevent [MASK] tokens from occupying a separate representation subspace from real tokens; exploring new self-supervised objectives that do not require using artificial tokens like [MASK]; and removing/reducing the need for an auxiliary decoder in pretraining which does not get used in downstream tasks.

References

Baevski, A., Hsu, W.-N., Xu, Q., Babu, A., Gu, J., and Auli, M. data2vec: A general framework for self-supervised learning in speech, vision and language. In *ICML*, 2022.

Bao, H., Dong, L., Wei, F., Wang, W., Yang, N., Liu, X., Wang, Y., Piao, S., Gao, J., Zhou, M., and Hon, H.-W. UniLMv2: Pseudo-masked language models for unified language model pre-training. In *ICML*, 2020.

Bao, H., Dong, L., and Wei, F. BEiT: BERT pre-training of image transformers. In *ICLR*, 2022.

Bender, E. M., Gebru, T., McMillan-Major, A., and Shmitchell, S. On the dangers of stochastic parrots: Can language models be too big? In *ACM Conference on Fairness, Accountability, and Transparency*, 2021.

Bentivogli, L., Clark, P., Dagan, I., and Giampiccolo, D. The fifth pascal recognizing textual entailment challenge. In *TAC*, 2009.

Bommasani, R., Hudson, D. A., Adeli, E., Altman, R., Arora, S., von Arx, S., Bernstein, M. S., Bohg, J., Bosselet, A., Brunskill, E., et al. On the opportunities and risks of foundation models. *ArXiv*, 2021.

Brown, T., Mann, B., Ryder, N., Subbiah, M., Kaplan, J. D., Dhariwal, P., Neelakantan, A., Shyam, P., Sastry, G., Askell, A., et al. Language models are few-shot learners. In *NeurIPS*, 2020.

Cai, X., Huang, J., Bian, Y., and Church, K. Isotropy in the contextual embedding space: Clusters and manifolds. In *ICLR*, 2021.

Cer, D., Diab, M., Agirre, E., Lopez-Gazpio, I., and Specia, L. Semeval-2017 task 1: Semantic textual similarity multilingual and crosslingual focused evaluation. In *International Workshop on Semantic Evaluation (SemEval)*, 2017.

Clark, K., Khandelwal, U., Levy, O., and Manning, C. D. What does BERT look at? an analysis of BERT’s attention. In *BlackboxNLP*, 2019.

Clark, K., Luong, M.-T., Le, Q. V., and Manning, C. D. ELECTRA: Pre-training text encoders as discriminators rather than generators. In *ICLR*, 2020.

Coenen, A., Reif, E., Yuan, A., Kim, B., Pearce, A., Viégas, F. B., and Wattenberg, M. Visualizing and measuring the geometry of BERT. In *NeurIPS*, 2019.

Dagan, I., Glickman, O., and Magnini, B. The pascal recognising textual entailment challenge. In *Machine Learning Challenges Workshop*, 2005.

Devlin, J., Chang, M.-W., Lee, K., and Toutanova, K. BERT: Pre-training of deep bidirectional transformers for language understanding. In *NAACL-HLT*, 2019.

Dodge, J., Marasović, A., Ilharco, G., Groeneveld, D., Mitchell, M., and Gardner, M. Documenting large web-text corpora: A case study on the colossal clean crawled corpus. In *EMNLP*, 2021.

Dolan, W. B. and Brockett, C. Automatically constructing a corpus of sentential paraphrases. In *International Workshop on Paraphrasing (IWP)*, 2005.

Dong, Y., Cordonnier, J.-B., and Loukas, A. Attention is not all you need: Pure attention loses rank doubly exponentially with depth. In *ICML*, 2021.

Dosovitskiy, A., Beyer, L., Kolesnikov, A., Weissenborn, D., Zhai, X., Unterthiner, T., Dehghani, M., Minderer, M., Heigold, G., Gelly, S., Uszkoreit, J., and Houlsby, N. An image is worth 16x16 words: Transformers for image recognition at scale. In *ICLR*, 2021.

Ethayarajh, K. How contextual are contextualized word representations? comparing the geometry of BERT, ELMo, and GPT-2 embeddings. In *EMNLP*, 2019.

Gao, J., He, D., Tan, X., Qin, T., Wang, L., and Liu, T.-Y. Representation degeneration problem in training natural language generation models. In *ICLR*, 2019.

Gao, T., Fisch, A., and Chen, D. Making pre-trained language models better few-shot learners. In *ACL*, 2021.

Giampiccolo, D., Magnini, B., Dagan, I., and Dolan, B. The third pascal recognizing textual entailment challenge. In *ACL-PASCAL workshop on textual entailment and paraphrasing*, 2007.

Gokaslan, A. and Cohen, V. OpenWebText corpus. <http://Skylion007.github.io/OpenWebTextCorpus>, 2019.

Goldberg, Y. Assessing BERT’s syntactic abilities. *ArXiv*, 2019.

Haim, R. B., Dagan, I., Dolan, B., Ferro, L., Giampiccolo, D., Magnini, B., and Szpektor, I. The second pascal recognising textual entailment challenge. In *PASCAL Challenges Workshop on Recognising Textual Entailment*, 2006.

He, K., Chen, X., Xie, S., Li, Y., Doll’ar, P., and Girshick, R. B. Masked autoencoders are scalable vision learners. In *CVPR*, 2022.

He, P., Gao, J., and Chen, W. DeBERTaV3: Improving DeBERTa using ELECTRA-style pre-training with gradient-disentangled embedding sharing. *ArXiv*, 2021a.

He, P., Liu, X., Gao, J., and Chen, W. DeBERTa: Decoding-enhanced BERT with disentangled attention. In *ICLR*, 2021b.

Hendrycks, D., Lee, K., and Mazeika, M. Using pre-training can improve model robustness and uncertainty. In *ICML*, 2019.

Hewitt, J. and Manning, C. D. A structural probe for finding syntax in word representations. In *NAACL*, 2019.

Hou, Z., Liu, X., Cen, Y., Dong, Y., Yang, H., Wang, C.-W., and Tang, J. GraphMAE: Self-supervised masked graph autoencoders. In *KDD*, 2022.

Joshi, M., Chen, D., Liu, Y., Weld, D. S., Zettlemoyer, L., and Levy, O. SpanBERT: Improving pre-training by representing and predicting spans. *Transactions of the Association for Computational Linguistics*, 8:64–77, 2019.

Ke, G., He, D., and Liu, T.-Y. Rethinking positional encoding in language pre-training. In *ICLR*, 2021.

Kumar, A., Raghunathan, A., Jones, R., Ma, T., and Liang, P. Fine-tuning can distort pretrained features and underperform out-of-distribution. In *ICLR*, 2022.

Lan, Z., Chen, M., Goodman, S., Gimpel, K., Sharma, P., and Soricut, R. ALBERT: A lite BERT for self-supervised learning of language representations. In *ICLR*, 2020.

Lewis, M., Liu, Y., Goyal, N., Ghazvininejad, M., Mohamed, A., Levy, O., Stoyanov, V., and Zettlemoyer, L. BART: Denoising sequence-to-sequence pre-training for natural language generation, translation, and comprehension. In *ACL*, 2020.

Li, B., Zhou, H., He, J., Wang, M., Yang, Y., and Li, L. On the sentence embeddings from pre-trained language models. In *EMNLP*, 2020.

Liang, P. P., Wu, C., Morency, L.-P., and Salakhutdinov, R. Towards understanding and mitigating social biases in language models. In *ICML*, 2021.

Liu, Y., Ott, M., Goyal, N., Du, J., Joshi, M., Chen, D., Levy, O., Lewis, M., Zettlemoyer, L., and Stoyanov, V. RoBERTa: A robustly optimized BERT pretraining approach. *ArXiv*, 2019.

Meng, Y., Xiong, C., Bajaj, P., Tiwary, S., Bennett, P., Han, J., and Song, X. COCO-LM: Correcting and contrasting text sequences for language model pretraining. In *NeurIPS*, 2021.

Meng, Y., Xiong, C., Bajaj, P., Tiwary, S., Bennett, P., Han, J., and Song, X. Pretraining text encoders with adversarial mixture of training signal generators. In *ICLR*, 2022.

Ott, M., Edunov, S., Baevski, A., Fan, A., Gross, S., Ng, N., Grangier, D., and Auli, M. FAIRSEQ: A fast, extensible toolkit for sequence modeling. In *NAACL-HLT Demonstrations*, 2019.

Radford, A., Narasimhan, K., Salimans, T., Sutskever, I., et al. Improving language understanding by generative pre-training. 2018.

Radford, A., Wu, J., Child, R., Luan, D., Amodei, D., and Sutskever, I. Language models are unsupervised multitask learners. *OpenAI blog*, 1(8):9, 2019.

Raffel, C., Shazeer, N., Roberts, A., Lee, K., Narang, S., Matena, M., Zhou, Y., Li, W., and Liu, P. J. Exploring the limits of transfer learning with a unified text-to-text transformer. *Journal of Machine Learning Research*, 2019.

Rajpurkar, P., Zhang, J., Lopyrev, K., and Liang, P. SQuAD: 100,000+ questions for machine comprehension of text. In *EMNLP*, 2016.

Sanh, V., Debut, L., Chaumond, J., and Wolf, T. DistilBERT, a distilled version of BERT: smaller, faster, cheaper and lighter. *ArXiv*, 2019.

Schick, T. and Schütze, H. Exploiting cloze-questions for few-shot text classification and natural language inference. In *EACL*, 2021.

Sennrich, R., Haddow, B., and Birch, A. Neural machine translation of rare words with subword units. In *ACL*, 2015.

Shankar, I., Nikhil, D., and Kornél, C. First Quora dataset release: Question pairs, 2017. URL <https://www.quora.com/q/quoradata/First-Quora-Dataset-Release-Question-Pairs>.

Socher, R., Perelygin, A., Wu, J., Chuang, J., Manning, C. D., Ng, A. Y., and Potts, C. Recursive deep models for semantic compositionality over a sentiment treebank. In *EMNLP*, 2013.

Tenney, I., Das, D., and Pavlick, E. BERT rediscovers the classical NLP pipeline. In *ACL*, 2019a.

Tenney, I., Xia, P., Chen, B., Wang, A., Poliak, A., McCoy, R. T., Kim, N., Durme, B. V., Bowman, S. R., Das, D., and Pavlick, E. What do you learn from context? probing for sentence structure in contextualized word representations. In *ICLR*, 2019b.

Tong, Z., Song, Y., Wang, J., and Wang, L. VideoMAE: Masked autoencoders are data-efficient learners for self-supervised video pre-training. In *NeurIPS*, 2022.

Trinh, T. H. and Le, Q. V. A simple method for common-sense reasoning. *ArXiv*, 2018.

Wang, A., Singh, A., Michael, J., Hill, F., Levy, O., and Bowman, S. R. GLUE: A multi-task benchmark and analysis platform for natural language understanding. In *EMNLP Workshop BlackboxNLP*, 2018.

Wang, R., Chen, D., Wu, Z., Chen, Y., Dai, X., Liu, M., Jiang, Y.-G., Zhou, L., and Yuan, L. BEVT: BERT pre-training of video transformers. In *CVPR*, 2022.

Warstadt, A., Singh, A., and Bowman, S. R. Neural network acceptability judgments. In *TACL*, 2019.

Wettig, A., Gao, T., Zhong, Z., and Chen, D. Should you mask 15% in masked language modeling? *ArXiv*, 2022.

Williams, A., Nangia, N., and Bowman, S. A broad-coverage challenge corpus for sentence understanding through inference. In *NAACL-HLT*, 2018.

Xie, Z., Zhang, Z., Cao, Y., Lin, Y., Bao, J., Yao, Z., Dai, Q., and Hu, H. SimMIM: a simple framework for masked image modeling. In *CVPR*, 2022.

Yang, Z., Dai, Z., Salakhutdinov, R., and Cohen, W. W. Breaking the softmax bottleneck: A high-rank rnn language model. In *ICLR*, 2018.

Yang, Z., Dai, Z., Yang, Y., Carbonell, J., Salakhutdinov, R. R., and Le, Q. V. XLNet: Generalized autoregressive pretraining for language understanding. In *NeurIPS*, 2019.

Zhu, Y., Kiros, R., Zemel, R., Salakhutdinov, R., Urtasun, R., Torralba, A., and Fidler, S. Aligning books and movies: Towards story-like visual explanations by watching movies and reading books. In *ICCV*, 2015.

A. Detailed Proofs

Theorem 2.2 (Rank deficiency of real token representations). *There exists some layer l in the Transformer encoder where the real token representation $\mathbf{H}_{\mathcal{R}}^l$ is rank-deficient. In particular, the row space of $\mathbf{H}_{\mathcal{R}}^l$ does not contain the row space of [MASK] token representation $\mathbf{H}_{\mathcal{M}}^l$.*

Proof. We prove the statement by contradiction: We suppose that the row space of $\mathbf{H}_{\mathcal{R}}^l$ always contains the row space of $\mathbf{H}_{\mathcal{M}}^l$ in all layers $1 \leq l \leq L$, and we will show that under this assumption, $\mathbf{H}_{\mathcal{M}}^l$ will converge exponentially (with l) to a rank-1 matrix, which contradicts with Lemma 2.1. We mainly analyze the rank change induced by the *self-attention* mechanism since it is the source of contextualization of [MASK] tokens (*i.e.*, the information exchange between [MASK] tokens and real tokens is achieved through self-attention). In the following, we assume *single-head* self-attention is used, and the analysis can be easily generalized to the multi-head case.

The self-attention module in the l th layer takes the previous layer representations \mathbf{H} (the superscript $l-1$ is omitted for convenience) as input and derives the output representations \mathbf{H}' :

$$\mathbf{H}' = \text{Attn}(\mathbf{H}\mathbf{W}^Q, \mathbf{H}\mathbf{W}^K, \mathbf{H}\mathbf{W}^V) \mathbf{W}^O = \text{Softmax}\left(\frac{\mathbf{H}\mathbf{W}^Q \mathbf{W}^{K^\top} \mathbf{H}^\top}{\sqrt{d}}\right) \mathbf{H}\mathbf{W}^V \mathbf{W}^O = \mathbf{A}\mathbf{H}\mathbf{W}^{VO},$$

where we denote the attention matrix computed from softmax as \mathbf{A} , and $\mathbf{W}^{VO} = \mathbf{W}^V \mathbf{W}^O$.

We study how the real token representations change (*i.e.*, comparing $\mathbf{H}'_{\mathcal{R}}$ with $\mathbf{H}_{\mathcal{R}}$) through the self-attention module. To facilitate easy analyses, we partition the input token representation matrix $\mathbf{H} \in \mathbb{R}^{(n+m) \times d}$ into blocks consisting of real token representations $\mathbf{H}_{\mathcal{R}} \in \mathbb{R}^{n \times d}$ and [MASK] token representations $\mathbf{H}_{\mathcal{M}} \in \mathbb{R}^{m \times d}$, and partition the attention matrix $\mathbf{A}_{\mathcal{R}}$ into blocks consisting of attention weights from real tokens to real tokens $\mathbf{A}_{\mathcal{R}:\mathcal{R}} \in \mathbb{R}^{n \times n}$ and from real tokens to [MASK] tokens $\mathbf{A}_{\mathcal{R}:\mathcal{M}} \in \mathbb{R}^{n \times m}$:

$$\mathbf{H} = \begin{bmatrix} \mathbf{H}_{\mathcal{R}} \\ \mathbf{H}_{\mathcal{M}} \end{bmatrix}, \quad \mathbf{A}_{\mathcal{R}} = [\mathbf{A}_{\mathcal{R}:\mathcal{R}} \quad \mathbf{A}_{\mathcal{R}:\mathcal{M}}].$$

We further denote

$$\mathbf{S}_{\mathcal{R}:\mathcal{R}} = \exp[\mathbf{H}_{\mathcal{R}} \mathbf{W}^{QK} \mathbf{H}_{\mathcal{R}}^\top], \quad \mathbf{S}_{\mathcal{R}:\mathcal{M}} = \exp[\mathbf{H}_{\mathcal{R}} \mathbf{W}^{QK} \mathbf{H}_{\mathcal{M}}^\top], \quad \mathbf{Z} = \text{diag}(\mathbf{S}_{\mathcal{R}:\mathcal{R}} \mathbf{1} + \mathbf{S}_{\mathcal{R}:\mathcal{M}} \mathbf{1}),$$

where $\exp[\cdot]$ denotes the element-wise exponential function, $\text{diag}(\cdot)$ constructs a diagonal matrix from a vector, $\mathbf{W}^{QK} = \mathbf{W}^Q \mathbf{W}^{K^\top} / \sqrt{d}$, and $\mathbf{1}$ is a vector of all ones. Then

$$\mathbf{A}_{\mathcal{R}:\mathcal{R}} = \mathbf{Z}^{-1} \mathbf{S}_{\mathcal{R}:\mathcal{R}}, \quad \mathbf{A}_{\mathcal{R}:\mathcal{M}} = \mathbf{Z}^{-1} \mathbf{S}_{\mathcal{R}:\mathcal{M}}.$$

Based on the above notations, the output representations at real token positions $\mathbf{H}'_{\mathcal{R}}$ can be written as:

$$\mathbf{H}'_{\mathcal{R}} = \mathbf{A}_{\mathcal{R}} \mathbf{H} \mathbf{W}^{VO} = [\mathbf{A}_{\mathcal{R}:\mathcal{R}} \quad \mathbf{A}_{\mathcal{R}:\mathcal{M}}] \begin{bmatrix} \mathbf{H}_{\mathcal{R}} \\ \mathbf{H}_{\mathcal{M}} \end{bmatrix} \mathbf{W}^{VO} = \mathbf{Z}^{-1} (\mathbf{S}_{\mathcal{R}:\mathcal{R}} \mathbf{H}_{\mathcal{R}} + \mathbf{S}_{\mathcal{R}:\mathcal{M}} \mathbf{H}_{\mathcal{M}}) \mathbf{W}^{VO}. \quad (4)$$

If the row space of $\mathbf{H}_{\mathcal{R}}$ contains the row space of $\mathbf{H}_{\mathcal{M}}$, each row of $\mathbf{H}_{\mathcal{M}}$ can be represented as a linear combination of the rows in $\mathbf{H}_{\mathcal{R}}$:

$$\mathbf{H}_{\mathcal{M}} = \mathbf{U} \mathbf{H}_{\mathcal{R}},$$

where $\mathbf{U} \in \mathbb{R}^{m \times n}$ is the linear combination weight matrix. We can rescale the vector norm of each row in $\mathbf{H}_{\mathcal{M}}$ so that \mathbf{U} has a row sum of one (*i.e.*, $\mathbf{U}\mathbf{1} = \mathbf{1}$).

To examine the rank of real token representations, we adopt a similar procedure as (Dong et al., 2021). We define the following residual \mathbf{R} which measures the difference between $\mathbf{H}_{\mathcal{R}}$ and a rank-1 matrix:

$$\mathbf{R} = \mathbf{H}_{\mathcal{R}} - \mathbf{1}\mathbf{h}^\top, \quad \mathbf{h} = \arg \min_{\mathbf{x}} \|\mathbf{H}_{\mathcal{R}} - \mathbf{1}\mathbf{x}^\top\|.$$

We aim to show that the norm of \mathbf{R} converges exponentially (with layer depth) to zero, meaning that $\mathbf{H}_{\mathcal{R}}$ converges (with layer depth) to a rank-1 matrix.

By plugging $\mathbf{H}_{\mathcal{R}} = \mathbf{R} + \mathbf{1}\mathbf{h}^\top$ and $\mathbf{H}_{\mathcal{M}} = \mathbf{U}\mathbf{H}_{\mathcal{R}} = \mathbf{U}\mathbf{R} + \mathbf{U}\mathbf{1}\mathbf{h}^\top = \mathbf{U}\mathbf{R} + \mathbf{1}\mathbf{h}^\top$ into Eq. (4), we obtain

$$\begin{aligned}\mathbf{H}'_{\mathcal{R}} &= \mathbf{Z}^{-1} (\mathbf{S}_{\mathcal{R}:\mathcal{R}} (\mathbf{R} + \mathbf{1}\mathbf{h}^\top) + \mathbf{S}_{\mathcal{R}:\mathcal{M}} (\mathbf{U}\mathbf{R} + \mathbf{1}\mathbf{h}^\top)) \mathbf{W}^{VO} \\ &= \left(\mathbf{Z}^{-1} (\mathbf{S}_{\mathcal{R}:\mathcal{R}} + \mathbf{S}_{\mathcal{R}:\mathcal{M}} \mathbf{U}) \mathbf{R} + \underbrace{\mathbf{Z}^{-1} (\mathbf{S}_{\mathcal{R}:\mathcal{R}} \mathbf{1} + \mathbf{S}_{\mathcal{R}:\mathcal{M}} \mathbf{1})}_{=1} \mathbf{h}^\top \right) \mathbf{W}^{VO} \\ &= \mathbf{Z}^{-1} (\mathbf{S}_{\mathcal{R}:\mathcal{R}} + \mathbf{S}_{\mathcal{R}:\mathcal{M}} \mathbf{U}) \mathbf{R} \mathbf{W}^{VO} + \mathbf{1}\mathbf{h}^\top \mathbf{W}^{VO}.\end{aligned}\tag{5}$$

Next we write out $\mathbf{S}_{\mathcal{R}:\mathcal{R}}$ and $\mathbf{S}_{\mathcal{R}:\mathcal{M}}$:

$$\begin{aligned}\mathbf{S}_{\mathcal{R}:\mathcal{R}} &= \exp [\mathbf{H}_{\mathcal{R}} \mathbf{W}^{QK} \mathbf{H}_{\mathcal{R}}^\top] \\ &= \exp [(\mathbf{R} + \mathbf{1}\mathbf{h}^\top) \mathbf{W}^{QK} (\mathbf{R} + \mathbf{1}\mathbf{h}^\top)^\top] \\ &= \exp [\mathbf{R} \mathbf{W}^{QK} \mathbf{R}^\top + \mathbf{1}\mathbf{h}^\top \mathbf{W}^{QK} \mathbf{R}^\top + (\mathbf{R} \mathbf{W}^{QK} \mathbf{h} + \mathbf{1}\mathbf{h}^\top \mathbf{W}^{QK} \mathbf{h}) \mathbf{1}^\top] \\ &= \exp \left[\underbrace{\mathbf{R} \mathbf{W}^{QK} \mathbf{R}^\top}_{=\mathbf{F}} \right] \odot \exp \left[\underbrace{\mathbf{1}\mathbf{h}^\top \mathbf{W}^{QK} \mathbf{R}^\top}_{=\mathbf{g}^\top} \right] \odot \exp \left[\underbrace{(\mathbf{R} \mathbf{W}^{QK} \mathbf{h} + \mathbf{1}\mathbf{h}^\top \mathbf{W}^{QK} \mathbf{h}) \mathbf{1}^\top}_{=\mathbf{c}} \right],\end{aligned}$$

and

$$\begin{aligned}\mathbf{S}_{\mathcal{R}:\mathcal{M}} &= \exp [\mathbf{H}_{\mathcal{R}} \mathbf{W}^{QK} \mathbf{H}_{\mathcal{M}}^\top] \\ &= \exp [(\mathbf{R} + \mathbf{1}\mathbf{h}^\top) \mathbf{W}^{QK} (\mathbf{U}\mathbf{R} + \mathbf{1}\mathbf{h}^\top)^\top] \\ &= \exp [\mathbf{R} \mathbf{W}^{QK} \mathbf{R}^\top \mathbf{U}^\top + \mathbf{1}\mathbf{h}^\top \mathbf{W}^{QK} \mathbf{R}^\top \mathbf{U}^\top + (\mathbf{R} \mathbf{W}^{QK} \mathbf{h} + \mathbf{1}\mathbf{h}^\top \mathbf{W}^{QK} \mathbf{h}) \mathbf{1}^\top] \\ &= \exp \left[\underbrace{\mathbf{R} \mathbf{W}^{QK} \mathbf{R}^\top \mathbf{U}^\top}_{=\mathbf{F}'} \right] \odot \exp \left[\underbrace{\mathbf{1}\mathbf{h}^\top \mathbf{W}^{QK} \mathbf{R}^\top \mathbf{U}^\top}_{=\mathbf{g}'^\top} \right] \odot \exp \left[\underbrace{(\mathbf{R} \mathbf{W}^{QK} \mathbf{h} + \mathbf{1}\mathbf{h}^\top \mathbf{W}^{QK} \mathbf{h}) \mathbf{1}^\top}_{=\mathbf{c}} \right],\end{aligned}$$

where \odot denotes the element-wise product. Let $\mathbf{F} = \mathbf{R} \mathbf{W}^{QK} \mathbf{R}^\top$, $\mathbf{F}' = \mathbf{R} \mathbf{W}^{QK} \mathbf{R}^\top \mathbf{U}^\top$, $\mathbf{g}^\top = \mathbf{h}^\top \mathbf{W}^{QK} \mathbf{R}^\top$, $\mathbf{g}'^\top = \mathbf{h}^\top \mathbf{W}^{QK} \mathbf{R}^\top \mathbf{U}^\top$, and $\mathbf{c} = \mathbf{R} \mathbf{W}^{QK} \mathbf{h} + \mathbf{1}\mathbf{h}^\top \mathbf{W}^{QK} \mathbf{h}$, we can further write out \mathbf{Z} :

$$\mathbf{Z} = \text{diag} (\mathbf{S}_{\mathcal{R}:\mathcal{R}} \mathbf{1} + \mathbf{S}_{\mathcal{R}:\mathcal{M}} \mathbf{1}) = \text{diag} (((\exp [\mathbf{F}] \odot \exp [\mathbf{1}\mathbf{g}^\top]) \mathbf{1} + (\exp [\mathbf{F}'] \odot \exp [\mathbf{1}\mathbf{g}'^\top]) \mathbf{1}) \odot \exp [\mathbf{c}]).$$

Let $\tilde{\mathbf{F}} = [\mathbf{F} \ \mathbf{F}']$ be the augmented matrix by combining the columns of \mathbf{F} and \mathbf{F}' , and let \bar{f}_i and \underline{f}_i denote the maximum and minimum element across each row of $\tilde{\mathbf{F}}$, respectively:

$$\bar{f}_i = \max_j \tilde{F}_{ij}, \quad \underline{f}_i = \min_j \tilde{F}_{ij}.$$

Then we can derive a lower bound of each element in $\mathbf{Z}^{-1} \mathbf{S}_{\mathcal{R}:\mathcal{R}}$:

$$\begin{aligned}[\mathbf{Z}^{-1} \mathbf{S}_{\mathcal{R}:\mathcal{R}}]_{ij} &= \frac{\exp(F_{ij}) \exp(g_j) \exp(c_i)}{\left(\sum_{j'} \exp(F_{ij'}) \exp(g_{j'}) + \sum_{j'} \exp(F'_{ij'}) \exp(g'_{j'}) \right) \exp(c_i)} \\ &\geq \frac{\exp(F_{ij}) \exp(g_j)}{\exp(\bar{f}_i) \left(\sum_{j'} \exp(g_{j'}) + \sum_{j'} \exp(g'_{j'}) \right)} \\ &= \exp(F_{ij} - \bar{f}_i) \frac{\exp(g_j)}{\sum_{j'} \exp(g_{j'}) + \sum_{j'} \exp(g'_{j'})}.\end{aligned}$$

Similarly, we can derive an upper bound:

$$[\mathbf{Z}^{-1} \mathbf{S}_{\mathcal{R}:\mathcal{R}}]_{ij} \leq \exp(F_{ij} - \underline{f}_i) \frac{\exp(g_j)}{\sum_{j'} \exp(g_{j'}) + \sum_{j'} \exp(g'_{j'})}.$$

Using the Taylor expansion of \exp , we have

$$\exp(F_{ij} - \bar{f}_i) \geq 1 + F_{ij} - \bar{f}_i \geq 1 + \underline{f}_i - \bar{f}_i, \quad \exp(F_{ij} - \underline{f}_i) \leq 1 + 2(F_{ij} - \underline{f}_i) \leq 1 + 2(\bar{f}_i - \underline{f}_i).$$

Therefore,

$$(1 + \underline{f}_i - \bar{f}_i) \frac{\exp(g_j)}{\sum_{j'} \exp(g_{j'}) + \sum_{j'} \exp(g'_{j'})} \leq [\mathbf{Z}^{-1} \mathbf{S}_{\mathcal{R}: \mathcal{R}}]_{ij} \leq (1 + 2\bar{f}_i - 2\underline{f}_i) \frac{\exp(g_j)}{\sum_{j'} \exp(g_{j'}) + \sum_{j'} \exp(g'_{j'})}.$$

Denote $\mathbf{D} = \text{diag}(\bar{f} - \underline{f})$ and $g_+ = \exp[\mathbf{g}^\top] \mathbf{1} + \exp[\mathbf{g}'^\top] \mathbf{1}$, then the above bound can be expressed in matrix form as follows (the inequality between matrices holds element-wise):

$$\frac{1}{g_+} (\mathbf{I} - \mathbf{D}) \mathbf{1} \exp[\mathbf{g}^\top] \leq \mathbf{Z}^{-1} \mathbf{S}_{\mathcal{R}: \mathcal{R}} \leq \frac{1}{g_+} (\mathbf{I} + 2\mathbf{D}) \mathbf{1} \exp[\mathbf{g}^\top]. \quad (6)$$

An analogous derivation gives the bound of $\mathbf{Z}^{-1} \mathbf{S}_{\mathcal{R}: \mathcal{M}}$:

$$\frac{1}{g_+} (\mathbf{I} - \mathbf{D}) \mathbf{1} \exp[\mathbf{g}'^\top] \leq \mathbf{Z}^{-1} \mathbf{S}_{\mathcal{R}: \mathcal{M}} \leq \frac{1}{g_+} (\mathbf{I} + 2\mathbf{D}) \mathbf{1} \exp[\mathbf{g}'^\top]. \quad (7)$$

Since the upper and lower bounds are in very similar forms, we will only focus on the upper bound in the derivations below.

Combining Eq. (6) with Eq. (7), we have

$$\begin{aligned} \mathbf{Z}^{-1} (\mathbf{S}_{\mathcal{R}: \mathcal{R}} + \mathbf{S}_{\mathcal{R}: \mathcal{M}} \mathbf{U}) &\leq \mathbf{1} \left(\underbrace{\frac{\exp[\mathbf{g}^\top] + \exp[\mathbf{g}'^\top] \mathbf{U}}{g_+}}_{= \mathbf{r}^\top} \right) + 2\mathbf{D} \mathbf{1} \left(\underbrace{\frac{\exp[\mathbf{g}^\top] + \exp[\mathbf{g}'^\top] \mathbf{U}}{g_+}}_{= \mathbf{r}^\top} \right) \\ &= \mathbf{1} \mathbf{r}^\top + 2\mathbf{D} \mathbf{1} \mathbf{r}^\top \end{aligned} \quad (8)$$

Plugging Eq. (8) into Eq. (5), we have

$$\mathbf{H}'_{\mathcal{R}} \leq (\mathbf{1} \mathbf{r}^\top + 2\mathbf{D} \mathbf{1} \mathbf{r}^\top) \mathbf{R} \mathbf{W}^{VO} + \mathbf{1} \mathbf{h}^\top \mathbf{W}^{VO} = \mathbf{1} \left(\underbrace{\mathbf{r}^\top \mathbf{R} \mathbf{W}^{VO} + \mathbf{h}^\top \mathbf{W}^{VO}}_{= \mathbf{h}'^\top} \right) + 2\mathbf{D} \mathbf{1} \mathbf{r}^\top \mathbf{R} \mathbf{W}^{VO}.$$

Therefore,

$$\mathbf{H}'_{\mathcal{R}} - \mathbf{1} \mathbf{h}'^\top \leq 2\mathbf{D} \mathbf{1} \mathbf{r}^\top \mathbf{R} \mathbf{W}^{VO}.$$

With a similar derivation, we have the following lower bound:

$$\mathbf{H}'_{\mathcal{R}} - \mathbf{1} \mathbf{h}'^\top \geq -\mathbf{D} \mathbf{1} \mathbf{r}^\top \mathbf{R} \mathbf{W}^{VO}.$$

Overall, we can bound the element-wise absolute values of $\mathbf{R}' = \mathbf{H}'_{\mathcal{R}} - \mathbf{1} \mathbf{h}'^\top$, which measure the distance between $\mathbf{H}'_{\mathcal{R}}$ and a rank-1 matrix:

$$|R'_{ij}| = \left| [\mathbf{H}'_{\mathcal{R}} - \mathbf{1} \mathbf{h}'^\top]_{ij} \right| \leq \left| [2\mathbf{D} \mathbf{1} \mathbf{r}^\top \mathbf{R} \mathbf{W}^{VO}]_{ij} \right|.$$

This allows us to further bound the norm of \mathbf{R}' . For ℓ_1 norm, we have

$$\begin{aligned} \|\mathbf{R}'\|_1 &\leq \|2\mathbf{D} \mathbf{1} \mathbf{r}^\top \mathbf{R} \mathbf{W}^{VO}\|_1 \\ &\leq 2 \|\mathbf{D} \mathbf{1}\|_\infty \|\mathbf{r}^\top \mathbf{R} \mathbf{W}^{VO}\|_1 && \text{Based on Hölder's inequality} \\ &\leq 2 \|\mathbf{D} \mathbf{1}\|_\infty \|\mathbf{r}^\top\|_1 \|\mathbf{R}\|_1 \|\mathbf{W}^{VO}\|_1, && \text{Submultiplicativity of matrix norms} \end{aligned}$$

where

$$\begin{aligned} \|\mathbf{D} \mathbf{1}\|_\infty &= \max_i |\bar{f}_i - \underline{f}_i| \\ &\leq 2 \|\tilde{\mathbf{F}}\|_1 \\ &\leq 2 \max \{ \|\mathbf{R} \mathbf{W}^{QK} \mathbf{R}^\top\|_1, \|\mathbf{R} \mathbf{W}^{QK} \mathbf{R}^\top \mathbf{U}^\top\|_1 \} \\ &\leq 2 \|\mathbf{R}\|_1 \|\mathbf{W}^{QK}\|_1 \|\mathbf{R}\|_\infty \max \{ 1, \|\mathbf{U}\|_\infty \} \\ &\leq 2 \|\mathbf{R}\|_1 \|\mathbf{W}^{QK}\|_1 \|\mathbf{R}\|_\infty \|\mathbf{U}\|_\infty, && \|\mathbf{U}\|_\infty \geq 1 \text{ since } \mathbf{U} \mathbf{1} = \mathbf{1} \end{aligned}$$

and

$$\begin{aligned}
 \|\mathbf{r}^\top\|_1 &\leq \|\mathbf{r}^\top\|_\infty \\
 &= \left\| \frac{\exp[\mathbf{g}^\top] + \exp[\mathbf{g}'^\top] \mathbf{U}}{g_+} \right\|_\infty \\
 &\leq \left\| \frac{\exp[\mathbf{g}^\top]}{g_+} \right\|_\infty + \left\| \frac{\exp[\mathbf{g}'^\top] \mathbf{U}}{g_+} \right\|_\infty \\
 &\leq 1 + \|\mathbf{U}\|_\infty.
 \end{aligned}$$

Therefore, we can bound the ℓ_1 norm of $\|\mathbf{R}'\|_1$ as follows:

$$\|\mathbf{R}'\|_1 \leq 4 \|\mathbf{W}^{QK}\|_1 \|\mathbf{W}^{VO}\|_1 \|\mathbf{U}\|_\infty (1 + \|\mathbf{U}\|_\infty) \|\mathbf{R}\|_1^2 \|\mathbf{R}\|_\infty. \quad (9)$$

Similarly, we can obtain the bound for the ℓ_∞ norm of $\|\mathbf{R}'\|_1$:

$$\|\mathbf{R}'\|_\infty \leq 4 \|\mathbf{W}^{QK}\|_1 \|\mathbf{W}^{VO}\|_\infty \|\mathbf{U}\|_\infty (1 + \|\mathbf{U}\|_\infty) \|\mathbf{R}\|_1 \|\mathbf{R}\|_\infty. \quad (10)$$

Denote the geometric mean of $\|\mathbf{R}\|_1$ and $\|\mathbf{R}\|_\infty$ as $\|\mathbf{R}\|_{1,\infty} = \sqrt{\|\mathbf{R}\|_1 \|\mathbf{R}\|_\infty}$, then from Eq. (9) and Eq. (10), we have

$$\begin{aligned}
 \|\mathbf{R}'\|_{1,\infty} &\leq 4 \underbrace{\|\mathbf{W}^{QK}\|_1 \|\mathbf{W}^{VO}\|_{1,\infty} \|\mathbf{U}\|_\infty (1 + \|\mathbf{U}\|_\infty)}_{=\epsilon} \|\mathbf{R}\|_{1,\infty}^3 \\
 &= 4\epsilon \|\mathbf{R}\|_{1,\infty}^3.
 \end{aligned}$$

The above inequality reflects how the residual changes within one self-attention layer. Applying it recursively throughout all layers in an L -layer encoder, we have:

$$\|\mathbf{R}^L\|_{1,\infty} \leq (4\bar{\epsilon})^{\frac{3^L-1}{2}} \|\mathbf{R}^0\|_{1,\infty}^{3^L}, \quad \bar{\epsilon} = \max_l \epsilon^l,$$

where \mathbf{R}^L and \mathbf{R}^0 denote the residuals corresponding to the encoder's output real token representations $\mathbf{H}_{\mathcal{R}}^L$ and input real token representations $\mathbf{H}_{\mathcal{R}}^0$, respectively.

This demonstrates that the residual norms of real token representations converge exponentially (with layer depth) to zero. Hence, the real token representation matrix $\mathbf{H}_{\mathcal{R}}^L$ converges exponentially (with layer depth) to a rank-1 matrix. Since the row space of [MASK] token representations $\mathbf{H}_{\mathcal{M}}^L$ is contained by the row space of $\mathbf{H}_{\mathcal{R}}^L$, we have $\text{rank}(\mathbf{H}_{\mathcal{M}}^L) \leq \text{rank}(\mathbf{H}_{\mathcal{R}}^L)$, and $\mathbf{H}_{\mathcal{M}}^L$ will also converge exponentially (with layer depth) to a rank-1 matrix, which contradicts with Lemma 2.1. Finally, we conclude that the row space of $\mathbf{H}_{\mathcal{R}}^L$ must not contain the row space of $\mathbf{H}_{\mathcal{M}}^L$, which necessarily implies that $\mathbf{H}_{\mathcal{R}}^L$ is rank-deficient. \square

B. Details about GLUE Tasks

More details of all the GLUE tasks can be found as follows.

MNLI: The Multi-genre Natural Language Inference (Williams et al., 2018) task includes 393K training examples from crowdsourcing. The goal is to predict if a premise sentence entails, contradicts, or is neutral with respect to a given hypothesis sentence.

QQP: Question Pairs (Shankar et al., 2017) includes 364K training examples from the Quora question-answering website. The task is to determine if two given questions are semantically equivalent.

QNLI: Question Natural Language Inference includes 108K training examples derived from the Stanford Question Answering Dataset (SQuAD) (Rajpurkar et al., 2016). The task is to predict if a sentence contains the answer to a given question.

SST-2: Stanford Sentiment Treebank (Socher et al., 2013) includes 67K training examples on movie reviews with human annotations. The task is to determine if a given sentence has positive or negative sentiment.

CoLA: Corpus of Linguistic Acceptability (Warstadt et al., 2019) includes 8.5K training examples from books and journal articles on linguistic theory. The task is to determine if a given sentence is linguistically acceptable.

RTE: Recognizing Textual Entailment (Bentivogli et al., 2009; Dagan et al., 2005; Haim et al., 2006; Giampiccolo et al., 2007) includes 2.5K training examples from textual entailment challenges. The task is to predict if a premise sentence entails a given hypothesis sentence.

MRPC: Microsoft Research Paraphrase Corpus (Dolan & Brockett, 2005) includes 3.7K training examples collected from news sources. The task is to predict if two given sentences are semantically equivalent.

STS-B: Semantic Textual Similarity (Cer et al., 2017) includes 5.8K training examples collected from multiple sources on sentence pair semantic similarity annotated by humans. The task is to predict the semantic similarity of two sentences (based on a 1 to 5 scoring scale).

C. Implementation Details

Computation Environment. The experiments in this paper are conducted on 64 A100 GPUs.

Masking. For all pretraining settings, we apply 15% random masks to input sequences. We do not use the trick in conventional MLM (Devlin et al., 2019; Liu et al., 2019) that replaces 10% of [MASK] tokens with the original ones and another 10% with random tokens. We also experiment with higher masking rates (*e.g.*, 40%) which are shown to be beneficial in (Wettig et al., 2022) for training large models, but they do not yield better results than the default 15% masking rate in our experiments. This is probably because (Wettig et al., 2022) use an efficient pretraining recipe that is different from the standard pretraining setup, with a larger learning rate, a larger batch size, a shorter sequence length, and fewer training steps.

Position Embedding. We learn both absolute and relative position embeddings (Raffel et al., 2019) in the encoder, and only learn absolute position embeddings in the decoder.

Dropout. During the pretraining of MAE-LM, dropout is applied to the encoder but not the decoder, which we find to slightly improve stability.

D. Hyperparameter Settings

We report the detailed hyperparameters used for pretraining in Table 4. The hyperparameter search ranges of fine-tuning are shown in Tables 5 and 6 for GLUE and SQuAD 2.0, respectively.

For fair comparisons, the same set of hyperparameters (in both pretraining and fine-tuning) is used for MAE-LM, RoBERTa (Ours) and ablations. We follow previous pretraining studies (Liu et al., 2019) to report the medians of downstream task fine-tuning results under the same set of five different random seeds.

Table 4: Hyperparameters used in pretraining.

Hyperparameter	<i>base</i>	<i>base++</i>	<i>large++</i>
Max Steps	125K	2M	1M
Peak Learning Rate	5e-4	2e-4	1e-4
Batch Size	2048	2048	2048
Warm-Up Steps	10K	10K	10K
Sequence Length	512	512	512
Relative Position Encoding Buckets	32	64	128
Relative Position Encoding Max Distance	128	128	256
Adam ϵ	1e-6	1e-6	1e-6
Adam (β_1, β_2)	(0.9, 0.98)	(0.9, 0.98)	(0.9, 0.98)
Clip Norm	2.0	2.0	1.0
Dropout	0.1	0.1	0.1
Weight Decay	0.01	0.01	0.01

Table 5: Hyperparameter ranges searched for fine-tuning on GLUE. GLUE small tasks include CoLA, RTE, MRPC and STS-B. GLUE large tasks include MNLI, QQP, QNLI and SST-2.

Hyperparameter	GLUE Small Tasks Search Space	GLUE Large Tasks Search Space
Max Epochs	{2, 3, 5, 10}	{2, 3, 5}
Peak Learning Rate	<i>base/base++</i> : {2e-5, 3e-5, 4e-5, 5e-5} <i>large++</i> : {7e-6, 1e-5, 2e-5, 3e-5}	<i>base/base++</i> : {1e-5, 2e-5, 3e-5, 4e-5} <i>large++</i> : {5e-6, 7e-6, 1e-5, 2e-5}
Batch Size	{16, 32}	32
Warm-Up Proportion	{6%, 10%}	6%
Sequence Length	512	512
Adam ϵ	1e-6	1e-6
Adam (β_1, β_2)	(0.9, 0.98)	(0.9, 0.98)
Clip Norm	-	-
Dropout	0.1	0.1
Weight Decay	0.01	0.01

Table 6: Hyperparameter ranges searched for fine-tuning on SQuAD 2.0.

Hyperparameter	SQuAD 2.0 Search Space
Max Epochs	{2, 3}
Peak Learning Rate	<i>base/base++</i> : {2e-5, 3e-5, 4e-5, 5e-5} <i>large++</i> : {7e-6, 1e-5, 2e-5, 3e-5}
Batch Size	{16, 32}
Warm-Up Proportion	{6%, 10%}
Sequence Length	512
Adam ϵ	1e-6
Adam (β_1, β_2)	(0.9, 0.98)
Clip Norm	-
Dropout	0.1
Weight Decay	0.01